



OPEN

Numerical treatment and global error estimation for thermal electro-osmosis effect on non-Newtonian nanofluid flow with time periodic variations

O. S. Ahmed^{1✉}, N. T. Eldabe², M. Y. Abou-zeid², O. H. El-kalaawy¹ & S. M. Moawad¹

The essential purpose of this study is to discuss the impact of time-periodic variations on mixed convection heat transfer for MHD Eyring-Powell nanofluid. The fluid flows through a non-Darcy porous medium over an infinite vertical plate. The effects of viscous dissipation, Ohmic dissipation, electro-osmosis force, heat source, thermal radiation, Dufour feature, and chemical reaction are presumed. The system of partial differential equations which governs the problem is transformed into a system of non-linear algebraic equations and then an explicit finite difference approach is espoused to solve these nonlinear algebraic equations. The numerical results for the velocity, temperature, and nanoparticles concentration distributions are computed and displayed through a set of graphs. Also, the skin friction coefficient, reduced Nusselt number, and Sherwood number are computed numerically for various values of the physical parameters. It is found that the velocity becomes greater with an elevation in the value of the Helmholtz–Smoluchowski velocity. Meanwhile, it enlarges with rising in the value of the electro-osmotic parameter. The rise in the value of the thermal radiation parameter causes a dwindling influence on both temperature and nanoparticles concentration. Investigations of these effects together are very useful due to their important vital applications in various scientific fields, especially in medicine and medical industries, such as endoscopes, respirators, and diverse medical implementations, as nanoparticles can be utilized in the remedy of cancer tumors. Additionally, electroosmotic flow is important due to its ability to control fluid movement and enhance mass transport, making it valuable in various application such as sample separation, drug delivery, and DNA analysis, offering enhanced efficiency and sensitivity.

List of symbols

Roman symbols

a and b	Parameters of Eyring-Powell model
\bar{b}	Non-Darcian parameter
A	Chemical reaction parameter
B_o	Strength of uniform magnetic field
C	Nanoparticles concentration
C_E	Ergun constant
C_p	Specific heat at constant pressure
C_s	Concentration susceptibility
Da	Darcy number
D_f	Dufour number
D_B	Brownian diffusion coefficient
D_T	Thermophoretic diffusion coefficient
e	The electronic charge

¹Department of Mathematics and Computer Science, Faculty of Science, Beni-Suef University, Beni-Suef, Egypt. ²Department of Mathematics, Faculty of Education, Ain Shams University, Heliopolis, Cairo, Egypt. ✉email: drOla.Sayed@science.bsu.edu.eg

E_c	Eckert number
E_x	The electric field component
F_s	Forchheimer number
g_0	Gravity acceleration
k	Thermal conductivity
K	Permeability constant
K_B	Boltzmann constant
K_T	Thermal diffusion ratio
m	Chemical reaction order
m_e	The electroosmotic parameter
M	Magnetic parameter
n_0	Bulk nanoparticles concentration
n^+	The cations
n^-	The anions
N	Buoyancy ratio
N_b	Brownian motion parameter
N_t	The thermophoresis parameter
Pr	Prandtl number
q	The radiative heat flux
Q_0	Heat source parameter
R	The radiation parameter
Sc	Schmidt number
t	Time
T	Temperature of the fluid
T_{av}	The average temperature
T_m	The mean temperature
U_{HS}	Helmholtz Smoluchowski velocity
V_i	Velocity vector = $(u(y, t), 0, 0)$
Z_v	The charge balance

Greek symbols

$\hat{\alpha}$	Non dimensional parameter
β	Volumetric coefficient of thermal expansion
β^*	Volumetric of expansion with nanoparticles concentration
δ	Non dimensional parameter
$\bar{\epsilon}$	The dielectric permittivity
φ	The electric potential
γ	Non dimensional parameter
μ	Viscosity
ν	Kinematic viscosity
ω	Frequency of the oscillating plate
ρ	The fluid density
ρ	The fluid density
ρ_e	The total ionic energy density
σ	Electrical conductivity of the fluid
τ	Stress tensor in Eyring-Powell model
ξ	The mean of electric potential

Superscripts and subscripts

∞	Free stream condition
w	Wall or plate condition

Nanofluid is a traditional liquid consisting of small particles of a diameter lower than 100 nm. It can be defined as a kind of fluid having the distinctive ability to improve the fluid thermal properties. Nanofluids have many applications in medicine, industry, and engineering. Choi¹ tested that the thermal conductivity of the base fluid will be improved after adding a small amount of these nanoparticles. Tripathi et al.² studied on peristaltic flow of nanofluids, and they ensure that the nanofluids yield suppressed back flow compared with Newtonian fluids. MHD transport of a third-grade nanofluid through a porous medium in the presence of thermal diffusion and diffusion thermo effects is discussed by Eldabe et al.³. Mekheimer et al.⁴ analyzed the blood flow with gold nanoparticles in the catheter. The flow behavior of a pseudo-plastic fluid containing tri-hybrid nanoparticles within the suspension; the flow is in the presence of different external effects such as Buoyancy forces, heat generation and viscous dissipations is discussed by Sohail et al.⁵. Nazir et al.⁶ examined the flow characteristics of a hyperbolic tangent liquid, considering the incorporation of ternary hybrid nanoparticles; the study analyzed the flow under various influencing factors, including a non-Darcy porous medium, surface rotation, external magnetic field, heat generation, and viscous dissipations. Many researchers have studied nanofluids flow through different surfaces⁷⁻¹⁹.

The study of non-Newtonian fluids is considered to be highly significant in engineering and applied science fields. There are various rheological models which utilizing to analyze and display the features of flow and transfer of heat. Although this model presents considerable mathematical complexity, it has garnered significant attention due to several compelling factors. Firstly, its constitutive relationship is established empirically, providing a practical approach. Secondly, the Eyring-Powell model exhibits both Newtonian behavior under both low and high shear stresses, making it particularly noteworthy. This model in the presence of different external forces plays an essential role in natural and geophysical processes which include delivery of dampness and temperature over environmental pollution, damaging of crops due to freezing, underground energy transport, geothermal reservoirs, thermal insulation, and agricultural fields^{20–24}.

The phenomenon of both heat and mass transfer plays a significant role in various industrial and engineering processes, such as equipment power collectors, food processing, heat exchangers, damage of crops, refrigeration, and reservoir engineering in connection with the thermal recovery process. So, in literature, convective transport theories for heat and mass are utilized by several researchers. The flow phenomenon in this case is relatively complex because these processes are containing heat transfer in non-Darcy porous media. Moreover, in the study of the dynamics of hot and salty springs of a sea, Fourier²⁵ is the first who introduced the heat conduction law and heat transfer properties. The electromagnetic field and Biot number effects on non-Newtonian nanofluid flow with heat transfer through a non-Darcy porous medium are analyzed by Abouzeid²⁶. Ismael et al.²⁷ discussed the effect of temperature conditions, slip velocity, and entropy generation on MHD biviscosity micropolar nanofluid flow via a porous medium in a peristaltic channel. The flow of non-Newtonian fluid past a shrinking plate through a porous media with transferring heat and mass is explained by Eldabe et al.²⁸. Several investigators discussed the flow with the impact of heat transfer of nanofluid^{29–34}.

Electro-osmosis force (EOF) is due to the electrolyte solution flow under the effect of an external electric field on an ionized certain surface. The surface catches ions of the opposite sign from the electrolyte solution and holds the ions of the same sign to generate an electric double layer (EDL). In this case, electro-osmotic flow can be generated in combination with an electrolyte and an insulating solid. In addition, in natural unfiltered water, as well as buffered solutions, electro-osmotic flow can occur. The electro-osmosis external force is first studied by Reuss³⁵. MHD peristaltic flow of Jeffery fluid through micro annulus in the presence of electro-osmosis force was studied by Mekheimer et al.³⁶. Nadeem et al.³⁷ observed electro-osmosis force on the microvascular blood flow. The electro-osmosis force and chemical reaction effects on the peristaltic flow of non-Newtonian nanofluid are focused on by Hegazy et al.³⁸.

As stated by the above studies, the fundamental target of this study is to describe the impacts of time-periodic variations as well as electro-osmosis forces on the flow of Eyring-Powell nanofluid through a non-Darcy porous media. The fluid is flowing past an infinite vertical plate under the effects of viscous dissipation, Soret with Dufour impacts, chemical reaction, and heat source. We transform the system of non-linear partial differential equations which govern the problem into algebraic non-linear equations by using the explicit finite difference method. Then, the numerical formulas for the velocity, temperature, and nanoparticles concentration as well as the skin friction, reduced Nusselt number, and Sherwood number are obtained. The influences of diverse physical parameters on the various distributions are computed numerically and displayed through a set of graphs. The computed numerical results are given using tables for parameters of engineering importance. Furthermore, there is a strong correlation seen between the current solutions and the earlier stated outcomes in the relevant circumstances. Physically, nanofluids have several implementations in diverse scientific fields like the medical industry; medicine. For example, some nanoparticles are utilized in the therapy of cancer tumors. Additionally, the current study will serve as a vehicle for understanding more complex problems in industry, engineering such as separation processes, flow tracers, polishing of prosthetic heart valves, reducing friction in oil pipelines, cooling of metallic plates, and other fields.

Mathematical formulation

Eyring-Powell model^{13,20} is chosen to describe the non-Newtonian fluid, which is in the usual notation given as:

$$\tau_{ij} = \left[\mu + \frac{1}{b} \sinh^{-1} \left(\frac{1}{a} \right) \right] \frac{\partial V_i}{\partial x_j}, \quad (1)$$

where $\tau_{xx} = 2\mu \frac{\partial u}{\partial x} + \frac{1}{b} \sinh^{-1} \left(\frac{2}{a} \frac{\partial u}{\partial x} \right)$,

$$\tau_{xy} = \tau_{yx} = \mu \left(\frac{\partial u}{\partial y} + \frac{\partial v}{\partial x} \right) + \frac{1}{b} \sinh^{-1} \left(\frac{1}{a} \left(\frac{\partial u}{\partial y} + \frac{\partial v}{\partial x} \right) \right),$$

$$\tau_{yy} = 2\mu \frac{\partial v}{\partial y} + \frac{1}{b} \sinh^{-1} \left(\frac{2}{a} \frac{\partial v}{\partial y} \right).$$

Consider the infinite vertical plate entrenched in an incompressible fluid (see Fig. 1). Initially, the temperature and nanoparticles concentration of both are assumed at T_∞ and C_∞ . Then, at $t > 0$, the plate temperature and nanoparticles concentration are elevated to T_ω and C_ω , and a periodic temperature and nanoparticles concentration are assumed. A uniform magnetic field B_0 is applied transversally to the flow. We choose any point of the flat vertical infinite plate to be the origin of the coordinate system, the x -axis is chosen along the vertical plate vertically upwards, and the y -axis perpendicular to the plate. The following set of differential equations can be written by using boundary-layer assumptions as^{6,8,13,20,29}:

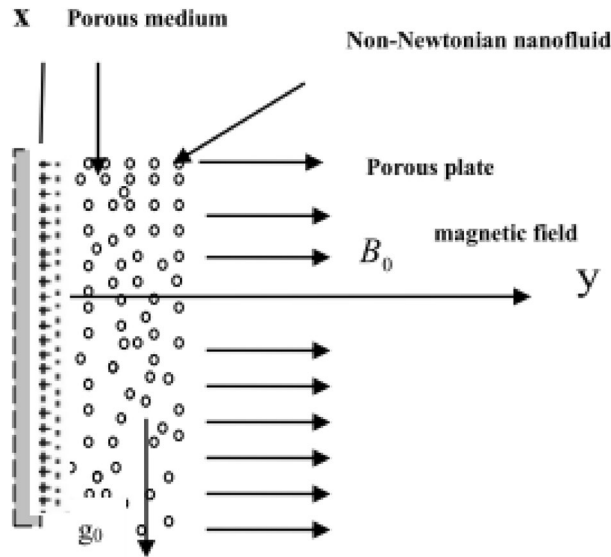


Figure 1. Sketch of the problem.

$$\frac{\partial u}{\partial t} = \nu \frac{\partial^2 u}{\partial y^2} + \frac{1}{\rho a b} \left(\frac{\partial^2 u}{\partial y^2} \right) \frac{1}{\sqrt{\frac{1}{a^2} \left(\frac{\partial u}{\partial y} \right)^2 + 1}} - \left(\frac{\sigma B_0^2}{\rho} + \frac{\nu}{K} \right) u - \bar{b} u^2 + \rho_e E_x + g_0 \beta (T - T_\infty) + g_0 \beta^* (C - C_\infty), \tag{2}$$

$$\begin{aligned} \frac{\partial T}{\partial t} = & \frac{k}{\rho C_p} \frac{\partial^2 T}{\partial y^2} + \frac{\nu}{C_p} \left(\frac{\partial u}{\partial y} \right)^2 + \frac{1}{\rho b C_p} \left(\frac{\partial u}{\partial y} \right) \sinh^{-1} \left(\frac{1}{a} \frac{\partial u}{\partial y} \right) + \nabla \cdot \underline{q} \\ & + \frac{\sigma B_0^2 u^2}{\rho C_p} + \frac{D_B K_T}{C_p C_s} \frac{\partial^2 C}{\partial y^2} + Q_0 (T - T_\infty) + D_B \left(\frac{\partial T}{\partial y} \frac{\partial C}{\partial y} \right) + D_T \left(\frac{\partial T}{\partial y} \right)^2, \end{aligned} \tag{3}$$

$$\frac{\partial C}{\partial t} = D_B \frac{\partial^2 C}{\partial y^2} + \frac{D_T}{T_m} \frac{\partial^2 T}{\partial y^2} - A(C - C_\infty)^m. \tag{4}$$

The appropriate initial and boundary conditions of the above equations may be expressed as^{20,29}:

$$u = 0, \quad T = T_\infty, \quad C = C_\infty \quad \text{for all } t \leq 0, \tag{5a}$$

$$\begin{aligned} u = 0, \quad T = T_\infty + \varepsilon (T_\omega - T_\infty) \cos \omega t, \\ C = C_\infty + \varepsilon (C_\omega - C_\infty) \cos \omega t \quad \text{at } y = 0, \quad t > 0, \end{aligned} \tag{5b}$$

$$u \rightarrow 0, \quad T \rightarrow T_\infty, \quad C \rightarrow C_\infty \quad \text{as } y \rightarrow \infty, \quad t > 0, \tag{5c}$$

By using the Rosseland approximation³⁹, the radiative heat flux may be defined as:

$$q_y = \frac{-4\sigma^*}{3k_R} \frac{\partial T^4}{\partial y}. \tag{6}$$

The temperature differences within the flow are small such that T^4 may be expressed as a linear function of temperature. This is achieved by expanding T^4 in a Taylor series about T_m and omitting higher-order terms³⁹, one gets:

$$T^4 \approx 4T_m^3 T - 3T_m^4. \tag{7}$$

By applying Gaussian's law^{14,36-38}, one gets:

$$\nabla \cdot \underline{E} = \rho_e \bar{\varepsilon}, \tag{8}$$

We assume that the electric field is a conservative field^{14,36-38}, then

$$\underline{E} = -\nabla \varphi \text{ and therefore, } \nabla^2 \varphi = -\rho_e \bar{\varepsilon}, \tag{9}$$

By using the Boltzmann distribution^{14,36–38}, the net charge density can be written as:

$$\rho_e = -Z_v e (n^- - n^+), \tag{10}$$

$$n^\pm = n_0 e^{\mp \frac{e z_v}{k_B T_{av}} \varphi}, \tag{11}$$

According to the Debye–Hückel linearization principle $\frac{e z_v}{k_B T_{av}} \ll 1$, then, Eq. (10) became as follows:

$$\rho_e = \frac{\bar{\epsilon}}{\lambda_e^2} \varphi, \tag{12}$$

where $\lambda_e = \frac{1}{e z_v} \sqrt{\frac{\bar{\epsilon} k_B T_{av}}{2 n_0}}$. Then, according to boundary-layer assumption, Eq. (10) may be written as:

$$\frac{d^2 \varphi}{dy^2} = \frac{1}{\lambda_e^2} \varphi. \tag{13}$$

Let us introduce the following dimensionless quantities^{6,13,14,20,29}:

$$t^* = \frac{t}{t_R}, \quad \omega^* = t_R \omega, \quad y^* = \frac{y}{L_R}, \quad u^* = \frac{u}{u_R}, \quad T^* = \frac{T - T_\infty}{T_\omega - T_\infty}, \quad C^* = \frac{C - C_\infty}{C_\omega - C_\infty}, \quad \varphi^* = \frac{\varphi}{\xi}, \tag{14}$$

$$\text{where } u_R = (\nu g_0 \beta \Delta T)^{\frac{1}{3}}, \quad L_R = \left(\frac{g_0 \beta \Delta T}{\nu^2} \right)^{-\frac{1}{3}} \text{ and } t_R = (g_0 \beta \Delta T)^{-\frac{2}{3}} \nu^{\frac{1}{3}}. \tag{15}$$

Then, Eq. (13) may be expressed as:

$$\frac{d^2 \varphi}{dy^2} = m_e^2 \varphi. \tag{16}$$

By applying the boundary conditions $\varphi = 1$ at $y = 0$ and $\varphi \rightarrow 0$ at $y \rightarrow \infty$, the analytical solution of Eq. (16) may be expressed as:

$$\varphi = e^{-m_e y}. \tag{17}$$

Then, the system of Eqs. (2), (3) and (4) is obtained in the dimensionless form as follows, after dropping the star mark

$$\frac{\partial u}{\partial t} = \left(1 + \frac{\hat{\alpha}}{\sqrt{\gamma \left(\frac{\partial u}{\partial y} \right)^2 + 1}} \right) \frac{\partial^2 u}{\partial y^2} - \left(M + \frac{1}{Da} \right) u - Fs u^2 + U_{HS} m_e^2 e^{-m_e y} + T + N C, \tag{18}$$

$$\begin{aligned} \frac{\partial T}{\partial t} = & \frac{(3 + 4R)}{3 Pr} \frac{\partial^2 T}{\partial y^2} + Ec \left(\frac{\partial u}{\partial y} \right)^2 + \frac{Ec}{\delta} \left(\frac{\partial u}{\partial y} \right) \sinh^{-1} \left(\sqrt{\gamma} \frac{\partial u}{\partial y} \right) \\ & + M Ec u^2 + Q_0 T + Nb \left(\frac{\partial T}{\partial y} \frac{\partial C}{\partial y} \right) + Nt \left(\frac{\partial T}{\partial y} \right)^2 + Df \frac{\partial^2 C}{\partial y^2}, \end{aligned} \tag{19}$$

$$\frac{\partial C}{\partial t} = \frac{1}{Sc} \frac{\partial^2 C}{\partial y^2} + \frac{Nt}{Nb} \frac{\partial^2 T}{\partial y^2} - \delta C^m, \tag{20}$$

The initial and boundary conditions in the dimensionless form are

$$u = 0, \quad T = 0, \quad C = 0 \text{ for all } y, \quad t \leq 0, \tag{21a}$$

$$u = 0, \quad T = \varepsilon \cos \omega t, \quad C = \varepsilon \cos \omega t \text{ at } y = 0, \quad t > 0, \tag{21b}$$

$$\text{and } u \rightarrow 0, \quad T \rightarrow 0, \quad C \rightarrow 0 \text{ as } y \rightarrow \infty, \quad t > 0 \tag{21c}$$

The finite difference method

The governing Eqs. (18)–(20) and the boundary conditions (21a, 21b and 21c) are solved numerically by using a standard explicit finite–difference technique¹⁶. Here, we can write

$$\begin{aligned}
 \frac{\partial u}{\partial t} &= \frac{u_i^{n+1} - u_i^n}{\Delta \tau} + O(\Delta \tau), & \frac{\partial T}{\partial t} &= \frac{T_i^{n+1} - T_i^n}{\Delta \tau} + O(\Delta \tau), \\
 \frac{\partial C}{\partial t} &= \frac{C_i^{n+1} - C_i^n}{\Delta \tau} + O(\Delta \tau), & \frac{\partial u}{\partial y} &= \frac{u_{i+1}^n - u_i^n}{\Delta y} + O(\Delta y), \\
 \frac{\partial^2 u}{\partial y^2} &= \frac{u_{i+1}^n - 2u_i^n + u_{i-1}^n}{(\Delta y)^2} + O(\Delta y)^2, & & \\
 \frac{\partial^2 T}{\partial y^2} &= \frac{T_{i+1}^n - 2T_i^n + T_{i-1}^n}{(\Delta y)^2} + O(\Delta y)^2, & & \\
 \frac{\partial^2 C}{\partial y^2} &= \frac{C_{i+1}^n - 2C_i^n + C_{i-1}^n}{(\Delta y)^2} + O(\Delta y)^2, & &
 \end{aligned}
 \tag{22}$$

where the index i refers to y and the $\Delta y = h = 0.05$ and $\Delta \tau = 0.003$. According to the boundary conditions (21a, 21b and 21c), the Mathematica package is used to solve Eqs. (18), (19) and (20) numerically, then a Newton iteration method continues until either the goals specified by accuracy goal or precision goal are achieved and determine the velocity and uniform magnetic field as a function of y .

Consistency of the finite difference scheme. The term consistency, which is applied to a finite difference method, means that the procedure may in fact approximate the solution of the partial differential equation of the present problem and not the solution of any other partial differential equation. The consistency is measured in terms of the difference between a differential equation and a difference equation. For consistency of Eqs. (18), (19) and (20), we estimate

$$\begin{aligned}
 & \left\{ \frac{u_i^{n+1} - u_i^n}{\Delta \tau} - \left(\frac{u_{i+1}^n - 2u_i^n + u_{i-1}^n}{(\Delta y)^2} \right) \left(1 + \frac{\hat{\alpha}}{\sqrt{\gamma \left(\frac{u_{i+1}^n - u_i^n}{\Delta y} \right)^2 + 1}} \right) + \left(M + \frac{1}{Da} \right) u_i^n - Fs (u_i^n)^2 + \right. \\
 & U_{HS} m_e^2 e^{-m_e i \Delta y} - T_i^n - N C_i^n \left. \right\} - \left\{ \frac{\partial u}{\partial t} - \left(1 + \frac{\hat{\alpha}}{\sqrt{\gamma \left(\frac{\partial u}{\partial y} \right)^2 + 1}} \right) \frac{\partial^2 u}{\partial y^2} - \left(M + \frac{1}{Da} \right) u - \right. \\
 & \left. Fs u^2 + U_{HS} m_e^2 e^{-m_e y} + T + N C \right\}_{i,n} = O(\Delta \tau) + O(\Delta \eta),
 \end{aligned}
 \tag{23}$$

$$\begin{aligned}
 & \left\{ \frac{T_i^{n+1} - T_i^n}{\Delta \tau} - \frac{(3 + 4R)}{3 Pr} \left(\frac{T_{i+1}^n - 2T_i^n + T_{i-1}^n}{(\Delta y)^2} \right) - Ec \left(\frac{u_{i+1}^n - u_i^n}{\Delta y} \right)^2 - \frac{Ec}{\delta} \left(\frac{u_{i+1}^n - u_i^n}{\Delta y} \right) \times \right. \\
 & \sinh^{-1} \left(\sqrt{\gamma} \left(\frac{u_{i+1}^n - u_i^n}{\Delta y} \right) \right) - MEc (u_i^n)^2 - Q_0 T_i^n - Nb \left(\frac{T_{i+1}^n - T_i^n}{\Delta y} \times \frac{C_{i+1}^n - C_i^n}{\Delta y} \right) - \\
 & \left. - Nt \left(\frac{T_{i+1}^n - T_i^n}{\Delta y} \right)^2 - Df \left(\frac{C_{i+1}^n - 2C_i^n + C_{i-1}^n}{(\Delta y)^2} \right) \right\} - \left\{ \frac{\partial T}{\partial t} - \frac{(3 + 4R)}{3 Pr} \frac{\partial^2 T}{\partial y^2} - Ec \left(\frac{\partial u}{\partial y} \right)^2 - \right. \\
 & \left. \frac{Ec}{\delta} \left(\frac{\partial u}{\partial y} \right) \sinh^{-1} \left(\sqrt{\gamma} \frac{\partial u}{\partial y} \right) - MEc u^2 - Q_0 T - Nb \left(\frac{\partial T}{\partial y} \frac{\partial C}{\partial y} \right) - Nt \left(\frac{\partial T}{\partial y} \right)^2 - Df \frac{\partial^2 C}{\partial y^2} \right\} \\
 & = O(\Delta \tau) + O(\Delta y),
 \end{aligned}
 \tag{24}$$

$$\begin{aligned}
 & \left\{ \frac{C_i^{n+1} - C_i^n}{\Delta \tau} - \frac{1}{Sc} \left(\frac{C_{i+1}^n - 2C_i^n + C_{i-1}^n}{(\Delta y)^2} \right) - \frac{Nt}{Nb} \left(\frac{T_{i+1}^n - 2T_i^n + T_{i-1}^n}{(\Delta y)^2} \right) + \delta (C_i^n)^m \right\} \\
 & - \left\{ \frac{\partial C}{\partial t} - \frac{1}{Sc} \frac{\partial^2 C}{\partial y^2} - \frac{Nt}{Nb} \frac{\partial^2 T}{\partial y^2} + \delta C^m \right\} = O(\Delta \tau) + O(\Delta \eta).
 \end{aligned}
 \tag{25}$$

Here, R.H.S. of Eqs. (23), (24) and (25) represent truncation error as $\Delta \tau \rightarrow 0$ with $\Delta y \rightarrow 0$, the truncation error tends to zero. Hence our explicit scheme is consistent.

Global error estimation. We use Zadunaisky technique⁴, to calculate the global error estimation G. E. E., which can be explained in the following steps:

- (1) Interpolate the functions u_i^n, T_i^n and C_i^n with their first derivatives, where $(i = 1, 2, \dots, 6)$ from their values, name them P_i ($i = 1, 2, \dots, 6$), and interpolate the functions of u'', T'' and C'' , and name them as $R_1(y) = u'', R_2(y) = T'', R_3(y) = C''$.
- (2) Calculate the detect functions D_i ($i = 1, 2, \dots, 6$), which can be written as follows:

1. $D_1(y) = P'_1 - P_2 = 0, D_2(y) = P'_2 - R_1(y),$
2. $D_3(y) = P'_3 - P_4 = 0, D_4(y) = P'_4 - R_2(y),$
3. $D_5(y) = P'_5 - P_6 = 0, D_6(y) = P'_6 - R_3(y),$
- (3) Add the defect functions D_i ($i = 1, 2, \dots, 6$) to the original problems and replace every Y_i by another variable Z_i ($i = 1, 2, \dots, 6$).
- (4) Solve the pseudo -problem by the same method to get the solution $Z(z)$ whose elements Z_i ($i = 1, 2, \dots, 6$).
- (5) Calculate the global error from the relation $e_n = Z_n - P(z_n)$, ($n = 1, 2, \dots, 6$), where Z_n is the approximate solution of the pseudo -problem at the point z_n and $Z(z_n)$ is the exact solution of the pseudo -problem at z_n . Obviously, the exact solution of pseudo -problems is $Z(z_n) = P(z_n)$.
- (6) The values of the global error are presented in Table 1. This error is based on using 11 points to find the interpolating polynomials P_i ($i = 1, 2, \dots, 6$), of degree 10^4 .

In order to achieve the above task we use the Mathematica package 10.1.

The skin-friction, heat and mass transfer⁴⁰

The skin-friction coefficient, reduced Nusselt number and Sherwood number in the non-dimensional form can be written as:

$$\tau_w = \left[\frac{\partial^2 u}{\partial y^2} \left(1 + \frac{\alpha}{\sqrt{\gamma \left(\frac{\partial u}{\partial y} \right)^2 + 1}} \right) \right]_{y=0}, \quad (26)$$

$$Nu = - \left[\frac{\partial T}{\partial y} \right]_{y=0}, \quad (27)$$

$$Sh = - \left[\frac{\partial C}{\partial y} \right]_{y=0}. \quad (28)$$

We can write equations (26), (27) and (28) by using finite difference method as follows:

$$\tau_w = \left(\frac{u_2^n - 2u_1^n + u_0^n}{(\Delta y)^2} \right) \left(1 + \frac{\alpha}{\sqrt{\gamma \left(\frac{u_1^n - u_0^n}{\Delta y} \right)^2 + 1}} \right), \quad (29)$$

$$Nu = - \left(\frac{T_1^n - T_0^n}{\Delta y} \right), \quad (30)$$

$$Sh = - \left(\frac{C_1^n - C_0^n}{\Delta y} \right). \quad (31)$$

Results and discussion

In this section, we show the effects of the problem's physical parameters on the velocity of the fluid, temperature, nanoparticles concentration, skin friction coefficient, reduced Nusselt number, and Sherwood number. These impacts were evaluated by setting the following standard values:

$\omega = 0.005, \gamma = 0.4, \varepsilon = 0.05, M = 10, Da = 0.1, Fs = 0.5, Gr = 0.5, Pr = 2.5, Q = 5, Ec = 1, Sc = 1, Df = 0.05, Nb = 2.5, Nt = 3.5, U_{HS} = 2, R = 1, m = 1, \text{ and } \delta = 0.1.$

Global error estimation						
y	u	e_1	T	e_3	C	e_5
0	0	0	0.05	0	0.05	0
0.4	0.05786	0.290D-3	0.1215	0.500D-5	-0.0115	-0.100D-5
0.8	0.06072	0.400D-3	0.1351	0.700D-5	-0.0186	-0.500D-6
1.2	0.47400	0.400D-3	0.1084	0.700D-5	-0.0065	-0.500D-6
1.6	0.02607	0.290D-3	0.0605	0.500D-5	-0.0003	-0.100D-5
2	0	0	0	0	0	0

Table 1. The values of the global error estimation for the velocity, temperature and nanoparticles concentration.

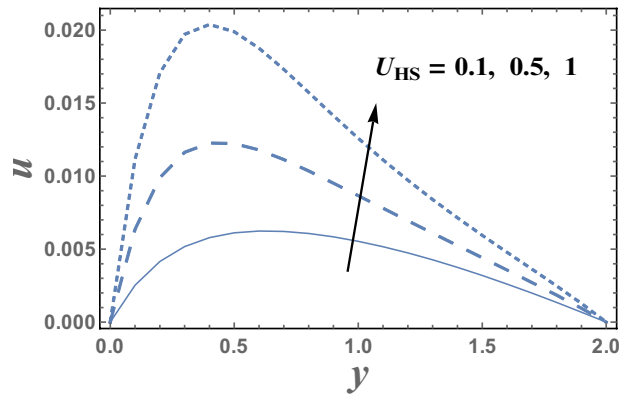


Figure 2. The velocity u is plotted with y , for different values of U_{HS} .

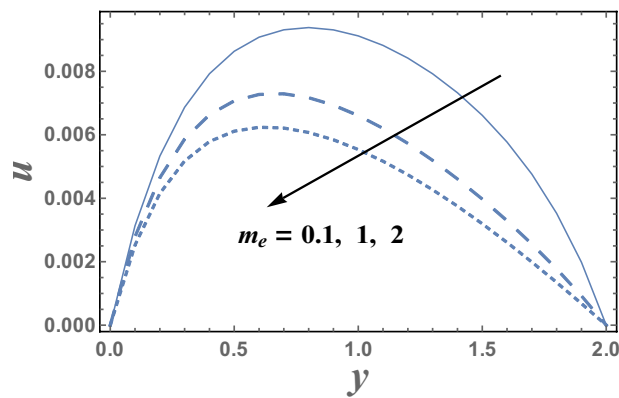


Figure 3. The velocity u is plotted with y , for different values of m_e .

Figures 2 and 3 are plotted to illustrate the influence of both the Helmholtz–Smoluchowski velocity dimensionless U_{HS} and the electro-osmotic parameter m_e on the velocity distribution $u(y)$. It is observed that the velocity distribution increases with an increase in the value of U_{HS} . Meanwhile, it decreases as m_e increases. Physically, Coulomb force induced by an electric field charges in a solution causes electro-osmotic flow. Because the chemical balance between a surface and an electrolyte solution usually leads to the interface acquiring a net fixed electrical charge, a layer of mobile ions, known as the Debye layer, creates in the region near the interface. When an electric field is applied to the fluid, the net charge in the electrical double layer is induced to move by the resulting Coulomb force. The resulting flow is termed electro-osmotic flow. So, the bigger resulting Coulomb

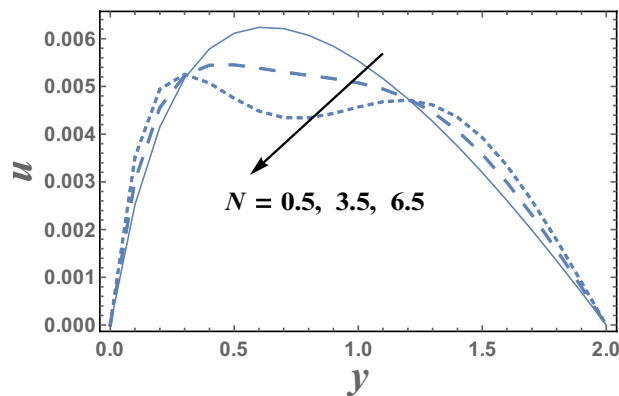


Figure 4. The velocity u is plotted with y , for different values of N .

force and consequently easily fluid flow. It is also noted that for each value of both U_{HS} and m_e , there exists a maximum value of u and all maximum values occur at $y \simeq 0.49$. Figure 4 illustrates the effect of the buoyancy ratio N on the velocity distribution u . It is found that the velocity increases with an enlargement in N in the intervals $y \in [0.0, 0.3] \cup [1.2, 2.0]$, otherwise it decreases by increasing N . So, the behavior of u in the interval $y \in [0.3, 1.2]$, is an inversed manner of its behavior in the other intervals. In this case, for each value of N , there are maximum values of u hold at $y = 0.65$. Figure 5 illustrates the impact of the thermophoresis parameter Nt on the velocity distribution $u(y)$. It depicts that in the interval of the coordinate $y \in [0.0, 1.29]$, the behavior of u for various values of Nt is exactly similar to the behavior of u for various values of m_e given in Fig. 3. It is also noted, from Fig. 5, that in the interval of the radial coordinate $y \in [1.29, 2.0]$, the behavior of u is an inversed manner of its behavior in the $y \in [0.0, 1.29]$ except that the curves are very close to each other in the second interval. Moreover, in the first interval, there is a maximum value of u holds at $y = 0.62$ and this maximum value slightly increases with an elevation in the value of Nt .

The variations of the temperature distribution T with the dimensionless coordinate y for various values of both Eckert number Ec and radiation parameter R are displayed throughout Figs. 6 and 7 respectively. The graphical results of Figs. 6 and 7 indicate that the temperature distribution T increases with an increase in the parameter Ec . From the physical point of view; during the motion of the fluid particles, the fluid viscosity converts some kinetic energy into thermal energy. This process is called viscous dissipation because it occurs due to viscosity. So, viscous dissipation can be defined as a heat source that results from the irreversible work done by the fluid flow to conquer the shear forces layers in the flow and appears as an increase in the fluid temperature. Consequently, it interprets the result in Fig. 6. This behavior is in agreement with that reported by^{40,41}. Meanwhile, it declines with an enhancement in the value of R . It is also noted that T increases with y till a definite value $y = y_0$ (represents the maximum value of T) and it decreases afterward. Similarly, we draw the variation of T with y for different values of the thermophoresis parameter D_f in Fig. 8, we will obtain a figure in which the behavior of the curves is the same as that obtained in Fig. 6, with the only difference that the obtained curves are very larger to each other than those obtained in Fig. 6. The results in Fig. 8, is due to the following; the Dufour effect is the energy flux due to a mass concentration gradient occurring as a coupled effect of irreversible processes. It is the reciprocal phenomenon to the Soret effect². The concentration gradient results in a temperature change. So, it always makes to increase the energy of fluids.

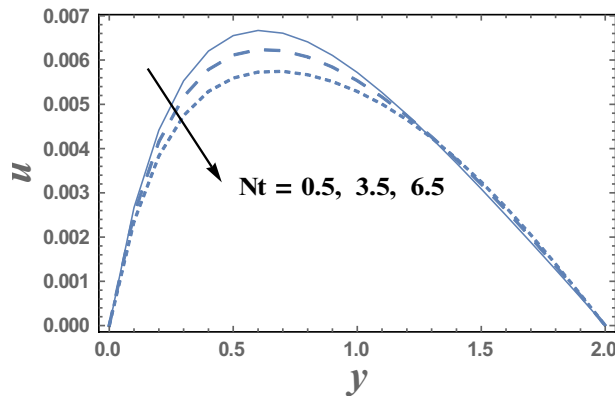


Figure 5. The velocity u is plotted with y , for different values of Nt .

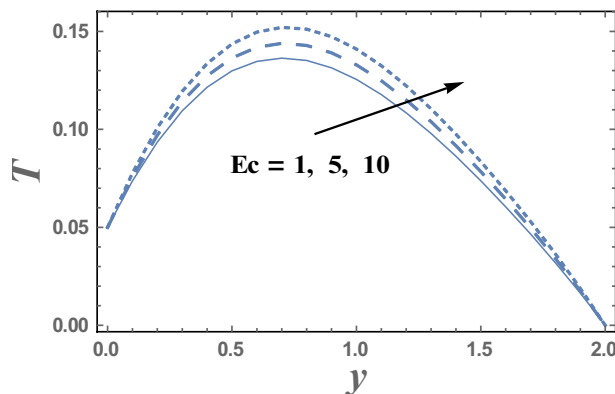


Figure 6. The temperature T is plotted with y , for different values of Ec .

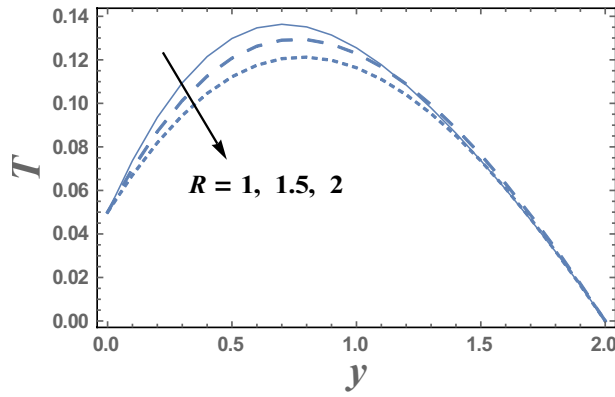


Figure 7. The temperature T is plotted with y , for different values of R .

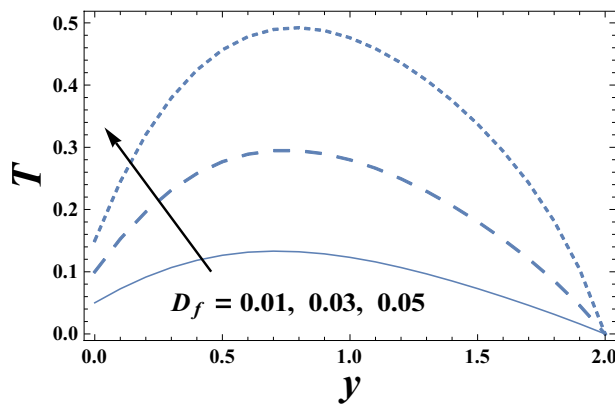


Figure 8. The temperature T is plotted with y , for different values of D_f .

Brownian motion as a natural phenomenon, is the random motion of particles suspended in a medium which may be a liquid or gas. This motion pattern typically consists of random fluctuations in a particle's position inside a fluid sub-domain, followed by a relocation to another sub-domain. Each relocation is followed by more fluctuations within the new closed volume. This pattern describes a fluid at thermal equilibrium and makes to increase the nanoparticles concentration. This will clarify the next result. Figures 9 and 10 represent the behaviors of the nanoparticles concentration distribution C with the dimensionless coordinate y for different values of Brownian motion parameter N_b and Dufour number D_f , respectively. It is observed from Figs. 9 and 10, that the nanoparticles concentration enhances with the increase of N_b . Whereas it dwindles as D_f elevates, respectively. On the other hand, it had an inverse effect near the wall $y=0$, namely in the interval $y \in [0.0, 0.18]$. It is also noted that the difference of the nanoparticles concentration distribution C for different values of N_b

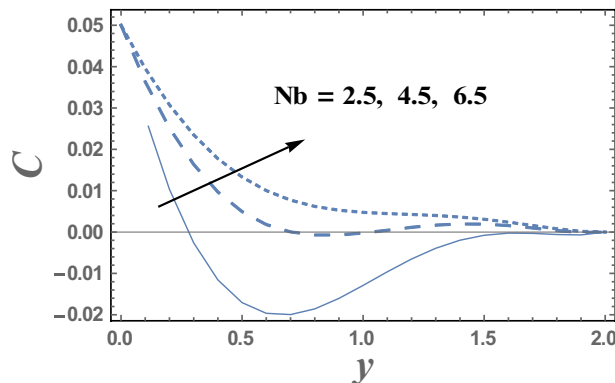


Figure 9. The nanoparticles concentration C is plotted with y , for different values of N_b .

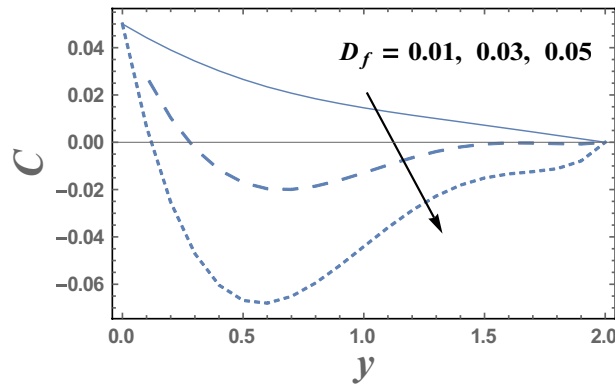


Figure 10. The nanoparticles concentration C is plotted with y , for different values of D_f .

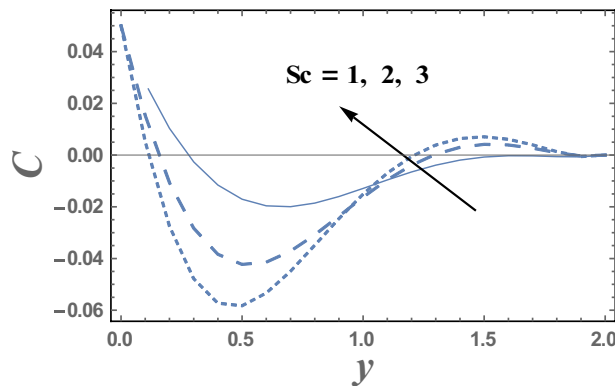


Figure 11. The nanoparticles concentration C is plotted with y , for different values of Sc .

and D_f , becomes lower with increasing the coordinate y and reaches minimum value, after which it increases. Figure 11 illustrates the effect of Schmidt number Sc on the nanoparticles concentration distribution C as a function of the dimensionless coordinate y . It is found that in the interval of the radial coordinate $y \in [0.0, 1.1]$, the behavior of C for various values of Sc is exactly similar to the behavior of C for various values of N_b given in Fig. 9. It is also noted, from Fig. 11 that in the interval of the coordinate $y \in [1.1, \infty)$, the behavior of C is an inversed manner of its behavior in the interval $y \in [0.0, 1.1]$, except that the curves are very close to each other in the first interval. In this case, for any value of the parameter Sc , there is a minimum value of C holds at $y = 0.49$, and this minimal slightly decreases by increasing the value of Sc . The influence of the thermal radiation parameter R on the nanoparticles concentration distribution C is illustrated in Fig. 12. It is found that the effect of R on C is opposite to the impact of Sc on C given in Fig. 11, with the only difference that, the curves in Fig. 11 are very close to those to each other in the first interval than those obtained in Fig. 12. Now, we will explicate how the radiation parameter affects the nanoparticles concentration. The thermal radiation parameter is defined as

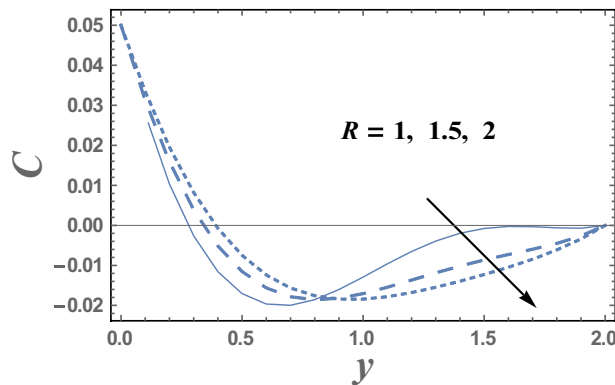


Figure 12. The nanoparticles concentration C is plotted with y , for different values of R .

the relative contribution of conduction heat transfer to thermal radiation transfer. It is evident that an increase in the radiation parameter causes in decreasing the nanoparticles concentration within the layer. The impacts of other parameters are similar to that obtained in Figs. 9 and 10. But, they are excluded here to avoid any kind of repetition.

Figures 13 and 14 illustrate the behavior of skin friction coefficient τ_ω with the time t , for various values of the electro-osmotic parameter m_e and Dufour number D_f . It is observed from these figures that skin friction coefficient increases as m_e increases, while it decreases with the increase of D_f . Moreover, we can notice from Figs. 13 and 14 that skin friction coefficient is always negative and decreases as t increases and at a finite value of t , the relation between τ_ω and t is a straight line parallel to the time.

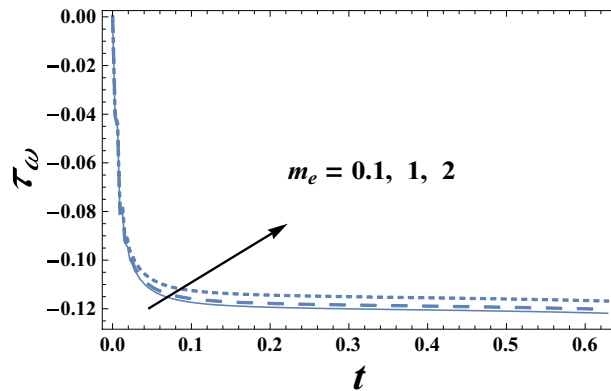


Figure 13. The skin friction coefficient τ_ω is plotted with t , for different values of m_e .

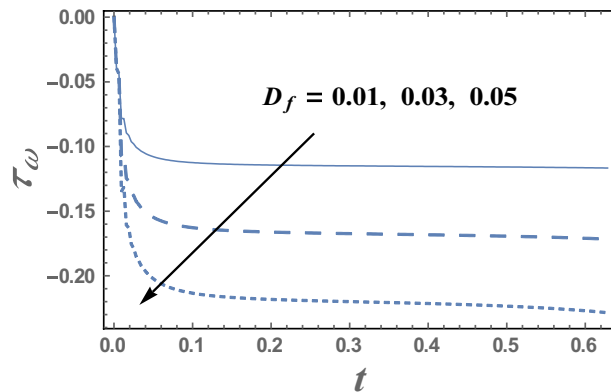


Figure 14. The skin friction coefficient τ_ω is plotted with t , for different values of D_f .

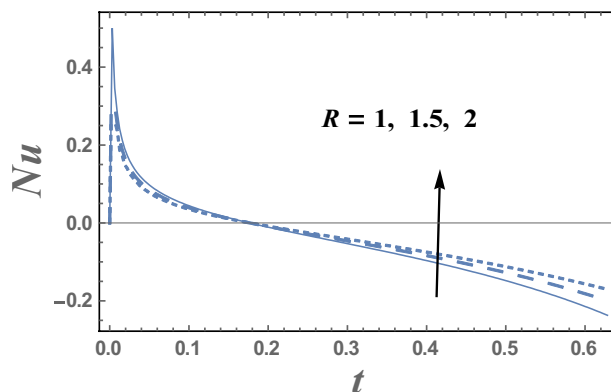


Figure 15. Nusselt number Nu is plotted with t , for different values of R .

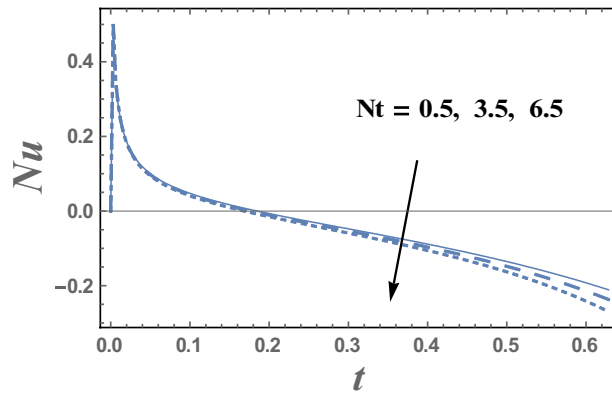


Figure 16. Nusselt number Nu is plotted with t , for different values of Nt .

The values of Nusselt number Nu are plotted versus the time t through Figs. 15 and 16 for various values of the thermal radiation parameter R and the thermophoresis parameter Nt . It is indicated from Figs. 15 and 16 that Nusselt number increases with increasing R and decreases with increasing values of R for $0 < t < 0.13$, while Nusselt number decreases as Nt increases. In addition, the values of Nu for different values of R and Nt , initially increases as t increases till a finite value of t , after which it crumbles.

The behavior of Sherwood number Sh with the time t for various values of Dufour number D_f , and the chemical reaction parameter δ are presented in Figs. 17 and 18, respectively. It is clear from these figures that Sherwood number decreases by increasing the chemical reaction parameter δ , while it increases by increasing Dufour number D_f . Moreover, it is noted that the difference of Sherwood number Sh for different values of γ ,

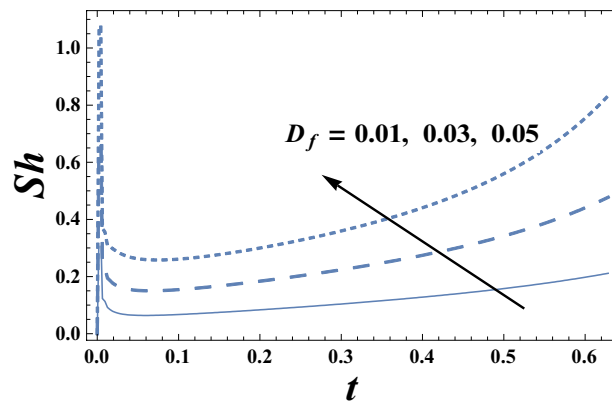


Figure 17. Sherwood number Sh is plotted with t , for different values of D_f .

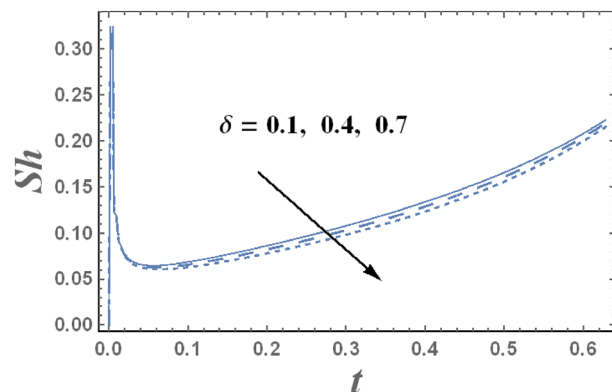


Figure 18. Sherwood number Sh is plotted with t , for different values of δ .

and Bn becomes lower with increasing t and reaches the minimum value, after which it increases. Note that the minimum value of Sherwood number decreases by increasing δ , whereas it increases with the increase of D_f . Further, it is found for each value of γ , $M Bn$ and, Sh is always positive.

Figures 19 and 20 display a comparison for the velocity and temperature values between our results and those obtained by B'eg et al.⁴². It is noticed that there is a good agreement in the obtained results.

Table 2 presents numerical results for the skin friction τ_ω , reduced Nusselt number Nu and Sherwood number Sh , for various values of the wave amplitude ε , Prandtl number Pr and heat source parameter Q_0 ⁴⁰. It is clear from Table 2, that an increase in ε , Pr and Q_0 gives an increase in the values of dimensionless quantity τ_ω and Sh , but decreasing in the dimensionless quantity Nu . In addition, these results have been compared with those obtained by B'eg et al.⁴², and it is found that there is a good agreement between our results and B'eg et al.⁴².

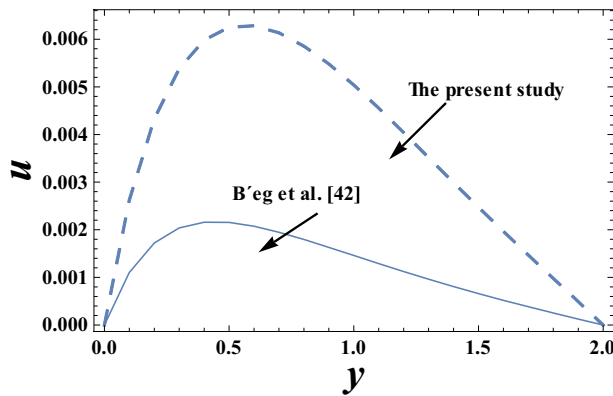


Figure 19. Comparison of the velocity values in our study and those obtained by B'eg et al.⁴².

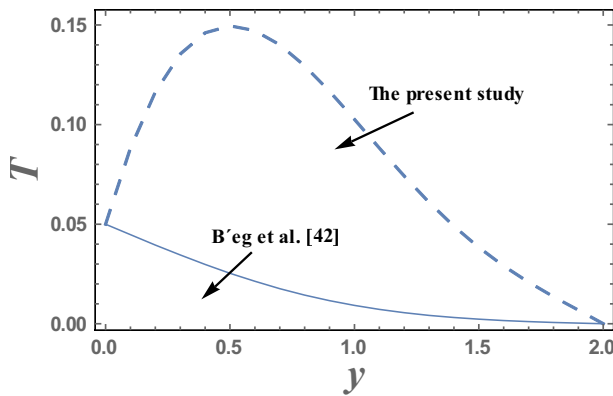


Figure 20. Comparison of the velocity values in our study and those obtained by B'eg et al.⁴².

ε	Pr	Q_0	τ_ω in the present study	τ_ω (B'eg et al. ⁴²)	Nu in the present study	Nu (B'eg et al. ⁴²)	Sh in the present study
0.05	2.5	1	0.0797		-0.0024		0.0066
0.1	2.5	1	0.1816		-0.0083		0.0821
0.2	2.5	1	0.6342		-0.1749		0.5998
0.2	3	1	0.2951	-0.1867	-0.0221	0.0957	0.2042
0.2	3.5	1	0.2954	-0.0891	-0.0320	0.0118	0.2166
0.2	4	1	0.2957	-0.0107	-0.0424	0.0083	0.2297
0.2	4	2	0.2290		-0.2348		0.4089
0.2	4	3	0.3047		-0.5515		0.6691
0.2	4	4	0.3169		-1.1642		1.1732

Table 2. Comparison between numerical results for the skin friction, reduced Nusselt number and Sherwood number in the present study and those obtained by B'eg et al.⁴².

Conclusion

The main target of this study is to present the effects of electro-osmosis forces on the free convective flow of Eyring-Powell nanofluid through a non-Darcy porous medium. The system is influenced by an external uniform magnetic field, thermal radiation, heat source, Ohmic dissipation, and viscous dissipation. The explicit-finite difference method is applied to obtain a numerical solution to the equations that govern the fluid motion. In addition, we obtain an estimation of the error propagation by using Zadunaisky technique for the finite difference method. The estimated errors ensure the usage of the approximated solutions as a suitable approximation to the calculated physical values. It is hoped that the present work will serve as a vehicle for understanding more complex problems in industry, engineering, and some physiological flows^{43–46}. The obtained results are also shown in a graphic representation and can be summarized as follows:

- (1) The velocity u decreases with an enrichment in ϵm_e , M , R , Sc and α . Whilst it elevates as Da , ϵ , Nb and Q_0 increase. In addition, as both N and Nt increase, it increases or dwindles.
- (2) By increasing the coordinate y , the velocity u for different values of problem physical parameters becomes greater and reaches a maximum value at a finite value, after which, it declines.
- (3) The temperature T increases with an enhancement in the values of Nt , Nb , Df , Q_0 and Ec . Whereas it dwindles or elevates as both R and Pr enhance.
- (4) All curves of the temperature for different values of the several physical parameters don't intersect at the plate $y = 0$, then increase as y escalates till a maximum value.
- (5) The behavior of nanoparticles concentration C seems to be opposite to the temperature behavior.

Future perspectives. Numerous potential applications in bioinformatics, fluid dynamics problems, and critically important financial mathematics may be numerically treated using the Lobatto IIIA and spectral collocation algorithms.

Data availability

The datasets generated and/or analyzed during the current study are not publicly available due [All the required data are only with the corresponding author] but are available from the corresponding author on reasonable request.

Received: 18 April 2023; Accepted: 29 August 2023

Published online: 08 September 2023

References

1. Choi, S. U. S. Enhancing thermal conductivity of fluids with nanoparticles. *ASME FED* **231**, 99–105 (1995).
2. Tripathi, D. & Beg, O. A. A study on peristaltic flow of nanofluids: Application in drug delivery systems. *Int. J. Heat Mass Transf.* **70**, 61–70 (2014).
3. Eldabe, N. T. M., Abou-zeid, M. Y., Abosaliem, A., Alana, A. & Hegazy, N. Thermal diffusion and diffusion thermo effects on magnetohydrodynamics transport of non-Newtonian nanofluid through a porous media between two wavy co-axial tubes. *IEEE Trans. Plasma Sci.* **50**, 1282–1290 (2021).
4. Abou-zeid, M. Y., Shaaban, A. A. & Alnour, M. Y. Numerical treatment and global error estimation of natural convective effects on gliding motion of bacteria on a power-law nanoslime through a non-Darcy porous medium. *J. Porous Media* **18**, 1091–1106 (2015).
5. Sohail, M. *et al.* A study of triple-mass diffusion species and energy transfer in Carreau-Yasuda material influenced by activation energy and heat source. *Sci. Rep.* **12**(1), 10219 (2022).
6. Nazir, U., Saleem, S., Al-Zubaidi, A., Shahzadi, I. & Feroz, N. Thermal and mass species transportation in tri-hybridized Sisko martial with heat source over vertical heated cylinder. *Int. Commun. Heat Mass Transf.* **134**, 106003 (2022).
7. Eldabe, N. T., Abou-zeid, M. Y., Mohamed, M. A. & Maged, M. Peristaltic flow of Herschel Bulkley nanofluid through a non-Darcy porous medium with heat transfer under slip condition. *Int. J. Appl. Electromagn. Mech.* **66**, 649–668 (2021).
8. Eldabe, N. T. M., Abou-zeid, M. Y., Elshabouri, S. M., Salama, T. N. & Ismael, A. M. Ohmic and viscous dissipation effects on micropolar non-Newtonian nanofluid Al_2O_3 flow through a non-Darcy porous media. *Int. J. Appl. Electromagn. Mech.* **68**, 209–221 (2022).
9. Eldabe, N. T. M., Abou-zeid, M. Y., Abosaliem, A., Alana, A. & Hegazy, N. Homotopy perturbation approach for Ohmic dissipation and mixed convection effects on non-Newtonian nanofluid flow between two co-axial tubes with peristalsis. *Int. J. Appl. Electromagn. Mech.* **67**, 153–163 (2021).
10. Ismael, A. M., Eldabe, N. T. M., Abou-zeid, M. Y. & Elshabouri, S. M. Thermal micropolar and couple stresses effects on peristaltic flow of biviscosity nanofluid through a porous medium. *Sci. Rep.* **12**, 16180 (2022).
11. Ouaf, M. E., Abou-Zeid, M. Y. & Younis, Y. M. Entropy generation and chemical reaction effects on MHD non-Newtonian nanofluid flow in a sinusoidal channel. *Int. J. Appl. Electromagn. Mech.* **69**, 45–65 (2022).
12. Ibrahim, M. G. & Abouzeid, M. Influence of variable velocity slip condition and activation energy on MHD peristaltic flow of Prandtl nanofluid through a non-uniform channel. *Sci. Rep.* **12**, 18747 (2022).
13. Basha, HTh. *et al.* Non-similar solutions and sensitivity analysis of nano-magnetic Eyring-Powell fluid flow over a circular cylinder with nonlinear convection. *Waves Random Complex Media* <https://doi.org/10.1080/17455030.2022.2128466> (2022).
14. Reddy, S. R. R., Basha, HTh. & Duraisamy, P. Entropy generation for peristaltic flow of gold-blood nanofluid driven by electrokinetic force in a microchannel. *Eur. Phys. J. Spec. Top.* **231**, 2409–2423 (2022).
15. Al-Mdallal, Q., Prasad, V. R., Basha, HTh., Sarris, I. & Akkurt, N. Keller box simulation of magnetic pseudoplastic nano-polymer coating flow over a circular cylinder with entropy optimization. *Comput. Math. Appl.* **118**, 132–158 (2022).
16. Basha, HTh., Rajagopal, K., Ahammad, N. A., Sathish, S. & Gunakala, S. R. Finite difference computation of Au-Cu/magneto-bio-hybrid nanofluid flow in an inclined uneven stenosis artery. *Complexity* **2022**, 1–18. <https://doi.org/10.1155/2022/2078372> (2022).
17. Basha, HTh. & Sivaraj, R. Exploring the heat transfer and entropy generation of Ag/FeO-blood nanofluid flow in a porous tube: A collocation solution. *Eur. Phys. J. Spec. Top.* **44**(31), 1–24 (2021).
18. Basha, HTh., Sivaraj, R. & Chamkha, A. J. SWCNH/diamond-ethylene glycol nanofluid flow over a wedge, plate and stagnation point with induced magnetic field and nonlinear radiation-solar energy application. *Eur. Phys. J. Spec. Top.* **228**, 2531–2551 (2019).

19. Arif, M., Suneetha, S., Basha, HTh., Reddy, P. B. A. & Kumam, P. Stability analysis of diamond-silver-ethylene glycol hybrid based radiative micropolar nanofluid: A solar thermal application. *Case Stud. Therm. Eng.* <https://doi.org/10.1016/j.csite.2022.102407> (2022).
20. Eldabe, N. T., Rizkallah, R. R., Abou-zeid, M. Y. & Ayad, V. M. Thermal diffusion and diffusion thermo effects of Eyring- Powell nanofluid flow with gyrotactic microorganisms through the boundary layer. *Heat Transf. Asian Res.* **49**, 383–405 (2020).
21. Eldabe, N. T., Rizkallah, R. R., Abou-zeid, M. Y. & Ayad, V. M. Effect of induced magnetic field on non-Newtonian nanofluid Al_2O_3 motion through boundary-layer with gyrotactic microorganisms. *Therm. Sci.* **26**, 411–422 (2022).
22. Eldabe, N. T., Moatimid, G. M., Abouzeid, M. Y., ElShekhipy, A. A. & Abdallah, N. F. A semianalytical technique for MHD peristalsis of pseudoplastic nanofluid with temperature- dependent viscosity: Application in drug delivery system. *Heat Transf. Asian Res.* **49**, 424–440 (2020).
23. Eldabe, N. T. M., Moatimid, G. M., Abou-zeid, M., Elshekhipy, A. A. & Abdallah, N. F. Instantaneous thermal-diffusion and diffusion-thermo effects on Carreau nanofluid flow over a stretching porous sheet. *J. Adv. Res. Fluid Mech. Therm. Sci.* **72**, 142–157 (2020).
24. Eldabe, N. T., Elshabouri, S., Elarabawy, H., Abouzeid, M. Y. & Abuiyada, A. J. Wall properties and Joule heating effects on MHD peristaltic transport of Bingham non-Newtonian nanofluid. *Int. J. Appl. Electromagn. Mech.* **69**, 87–106 (2022).
25. Fourier, J. B. *Theorieanalytique, De La Chaleur* Paris (1822).
26. Abouzeid, M. Y. Chemical reaction and non-Darcian effects on MHD generalized Newtonian nanofluid motion. *Egypt. J. Chem.* **65**(12), 647–655 (2022).
27. Ismael, A. M., Eldabe, N. T., Abouzeid, M. Y. & Elshabouri, S. Entropy generation and nanoparticles cu o effects on MHD peristaltic transport of micropolar non-newtonian fluid with velocity and temperature slip conditions. *Egypt. J. Chem.* **65**, 715–722 (2022).
28. Eldabe, N. T., Abou-zeid, M. Y., El-Kalaawy, O. H., Moawad, S. M. & Ahmed, O. S. Electromagnetic steady motion of Casson fluid with heat and mass transfer through porous medium past a shrinking surface. *Therm. Sci.* **25**(1A), 257–265 (2021).
29. Abou-zeid, M. Y. & Ouaf, M. E. Hall currents effect on squeezing flow of non-Newtonian nanofluid through a porous medium between two parallel plates. *Case Stud. Therm. Eng.* **28**, 10362 (2021).
30. El-Dabe, N. T., Abou-Zeid, M. Y. & Ahmed, O. S. Motion of a thin film of a fourth grade nanofluid with heat transfer down a vertical cylinder: Homotopy perturbation method application. *J. Adv. Res. Fluid Mech. Therm. Sci.* **66**, 101–113 (2020).
31. Ibrahim, M., Abdallah, N. & Abouzeid, M. Activation energy and chemical reaction effects on MHD Bingham nanofluid flow through a non-Darcy porous media. *J. Chem.* **65**(13B), 137–144 (2022).
32. Eldabe, N. T. M., Abouzeid, M. Y. & Ali, H. A. Effect of heat and mass transfer on Casson fluid flow between two co-axial tubes with peristalsis. *J. Adv. Res. Fluid Mech. Therm. Sci.* **76**(1), 54–75 (2020).
33. Eldabe, N. T., Abou-zeid, M. Y. & Shawky, H. A. MHD peristaltic transport of Bingham blood fluid with heat and mass transfer through a non-uniform channel. *J. Adv. Res. Fluid Mech. Therm. Sci.* **77**, 145–159 (2021).
34. Mansour, H. M. & Abou-zeid, M. Y. Heat and mass transfer effect on non-Newtonian fluid flow in a non-uniform vertical tube with peristalsis. *J. Adv. Res. Fluid Mech. Therm. Sci.* **61**(1), 44–62 (2019).
35. Reuss, F. F. *Mémoires de la Société Impériale Des Naturalistes de Moscou. Imp. Moscow Univ.* **2**, 327–337 (1809).
36. Mekheimer, K. S., Abo-Elkhaier, R. E. & Moawad, A. M. A. Electro-osmotic flow of non-Newtonian biofluids through wavy micro-concentric tubes. *Bionanoscience* **8**, 723–734 (2018).
37. Nadeem, S., Kiani, M. N., Saleem, A. & Issakhov, A. Microvascular blood flow with heat transfer in a wavy channel having electroosmotic effects. *Electrophoresis* **41**, 1198–1205 (2020).
38. Hegazy, N., Eldabe, N. T., Abouzeid, M., Abousaleem, A. & Alana, A. Influence of both chemical reaction and electro-osmosis on MHD non-Newtonian fluid flow with gold nanoparticles. *Egypt. J. Chem.* <https://doi.org/10.21608/EJCHEM.2023.190175.7526> (2023).
39. El-dabe, N. T. M. & Abou-zeid, M. Y. Radially varying magnetic field effect on peristaltic motion with heat and mass transfer of a non-Newtonian fluid between two co-axial tubes. *Therm. Sci.* **22**(6A), 2449–2458 (2018).
40. Abou-zeid, M. Y. Homotopy perturbation method to gliding motion of bacteria on a layer of power-law nanoslime with heat transfer. *J. Comput. Theor. Nanosci.* **12**, 3605–3614 (2015).
41. Eldabe, N. T., Hassan, M. A. & Abou-zeid, M. Y. Wall properties effect on the peristaltic motion of a coupled stress fluid with heat and mass transfer through a porous media. *J. Eng. Mech.* **142**, 04015102 (2016).
42. Anwar Beg, O., Zueco, J., Ghosh, S. K. & Heidari, A. Unsteady magnetohydrodynamic heat transfer in a semi-infinite porous medium with thermal radiation flux: Analytical and numerical study. *Adv. Numer. Anal.* **142**, 04015102 (2016).
43. Eldabe, N. T. M., Moatimid, G. M., Abou-zeid, M., Elshekhipy, A. A. & Abdallah, N. F. Semi-analytical treatment of Hall current effect on peristaltic flow of Jeffery nanofluid. *Int. J. Appl. Electromagn. Mech.* **7**, 47–66 (2021).
44. Eldabe, N. T. M., Abou-zeid, M. Y., Oauf, M. E., Mostapha, D. R. & ohamed, Y. M. Cattaneo-Christov heat flux effect on MHD peristaltic transport of Bingham nanofluid through a non-Darcy porous medium. *Int. J. Appl. Electromagn. Mech.* **68**, 59–84 (2022).
45. Sohail, M. *et al.* Finite element analysis for ternary hybrid nanoparticles on thermal enhancement in pseudo-plastic liquid through porous stretching sheet. *Sci. Rep.* **12**(1), 9219 (2022).
46. Nazir, U., Sohail, M., Hafeez, M. B. & Krawczuk, M. Significant production of thermal energy in partially ionized hyperbolic tangent material based on ternary hybrid nanomaterials. *Energies* **14**(21), 6911 (2021).

Acknowledgements

The authors 'd like to thank the reviewers for their valuable remarks which improved and enriched our manuscript.

Author contributions

O.S. Ahmed wrote the main manuscript text. O.H. El-kalaawy and S.M. Moawad prepared figures. N.T. Eldabe and M.Y. Abouzeid reviewed the manuscript.

Funding

Open access funding provided by The Science, Technology & Innovation Funding Authority (STDF) in cooperation with The Egyptian Knowledge Bank (EKB).

Competing interests

The authors declare no competing interests.

Additional information

Correspondence and requests for materials should be addressed to O.S.A.

Reprints and permissions information is available at www.nature.com/reprints.

Publisher's note Springer Nature remains neutral with regard to jurisdictional claims in published maps and institutional affiliations.



Open Access This article is licensed under a Creative Commons Attribution 4.0 International License, which permits use, sharing, adaptation, distribution and reproduction in any medium or format, as long as you give appropriate credit to the original author(s) and the source, provide a link to the Creative Commons licence, and indicate if changes were made. The images or other third party material in this article are included in the article's Creative Commons licence, unless indicated otherwise in a credit line to the material. If material is not included in the article's Creative Commons licence and your intended use is not permitted by statutory regulation or exceeds the permitted use, you will need to obtain permission directly from the copyright holder. To view a copy of this licence, visit <http://creativecommons.org/licenses/by/4.0/>.

© The Author(s) 2023